Adaptive winding pin and hooking capacity model for coreless filament winding

Pascal Mindermann[1] and **Götz T Gresser[1,2]**

Abstract

Coreless filament winding is a manufacturing process used for fiber-reinforced composites, resulting in high-performance lightweight lattice structures. Load transmission elements, which are assembled from commercially available standardized parts, often restrict the component design. A novel adaptive winding pin was developed, which is made by additive manufacturing and can therefore be adjusted to specific load conditions resulting from its position within the component. This allows to decouple the fiber arrangement from the winding pin orientation, which allows a fully volumetric framework design of components. A predictive model for the pin capacity was derived and experimentality validated. The hooking conditions, pin capacity, and occupancy were considered in the creation of a digital design tool.

Introduction

The cross-industry applications of fiber-reinforced composites for structural components with profile, planar, or shell shapes have been described in the literature.[1–5] The manufacturing process of coreless filament winding (CFW)[6,7] allows its utilization in shells[8] and lattice frameworks.[9] For technical applications where high specific mechanical properties are required, CFW offers a superior performance, since it allows for full control over the component geometry and fiber orientation.

Filament winding[10] is a manufacturing process that is often used for pressure tanks, in which impregnated rovings are continuously placed onto a cylindrical mandrel under persistent tension. The mandrel defines the shape[11] and surface quality of the produced composite, limits the design freedom, and increases the initial production cost. CFW evolved from this by removing the mandrel[12] and introducing spatially arranged point-like elements, called anchors, to place the fibers around them. Such anchors are held in place by a winding fixture, which can be shaped like a plate, frame, mold, or mandrel. The fibers do not touch the fixture, but if they do, it is considered a hybrid[13] CFW process. Fibers impregnated with thermoset resins are placed around the anchors in a specific order, the winding syntax.[14] The fibers often mechanically interact with each other during the winding process. This, the syntax, and the geometrical arrangement of the anchors largely define the shape and performance of the component.[15] After the winding is completed, the resin is cured with/without thermal treatment, depending on the resin formulation/component requirements. After curing, the fixture is removed for most applications.[16] In some cases, it remains in the component as part of the supporting structure.[17] Some part of the anchor almost always remains within the component as a load transmission element.

At present, many components realized in CFW are shell-shaped.[18] Apart from the design strategy,[19] where stiffness is created from shape, the reason why the often-used shell shape is used are the restrictions[20] of the anchor type deployed in the fiber arrangement. Moreover, recent utilizations[21,22] of CFW for construction have demonstrated an amount of deployed material that has caused separate fiber bundles to merge together and thus cause the lattice appearance to transition into a continuous shell. In order to exploit the full potential of CFW, a new anchor is needed to remove this limitation and allow the creation of volumetric, sparse, and fully stressed framework structures, which are more useful for engineering applications with dynamic load cases.[23] According to the state of the art, during the design

[1]Institute for Textile and Fiber Technologies, University of Stuttgart, Germany
[2]German Institutes of Textile and Fiber Research Denkendorf, Denkendorf, Germany

Corresponding author:
Pascal Mindermann, Institute for Textile and Fiber Technologies, University of Stuttgart, Pfaffenwaldring 9, 70569 Stuttgart, Germany.
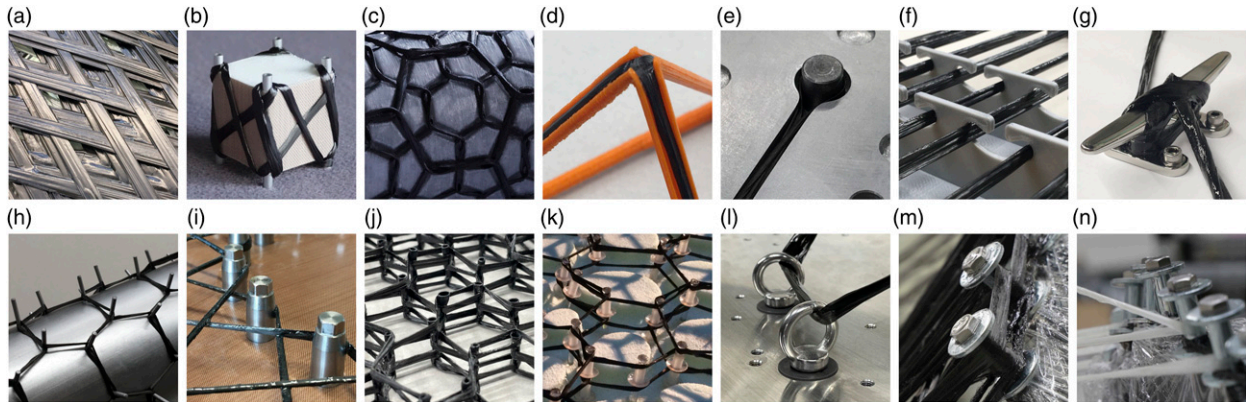Email: pascal.mindermann@itft.uni-stuttgart.de

Figure 1. State-of-the-art anchors used in CFW: (a) already-placed fiber bundles, (b) sleeves on water-soluble mold covered by PTFE foil, (c) nails (already removed) on mandrel with grooves, (d) grooves, (e) metallic cylinders and forming mold, (f) undercuts, (g) hooks (cleat-like elements), (h) spikes on cylindrical mandrel, (i) custom pins, (j) nails (already removed) with a heat shrink tube, (k) rivets on foam, (l) eyelets, (m) sleeve/washer winding pins on metallic frame, and (n) vertical fiber angle at winding pin.

process the capacity and occupancy of the winding pins were estimated based on the designer's experience or determined empirically, which caused design iterations. Formulas for calculating cable or robe drums[24] cannot be transferred to CFW due to the very different nature of the process.

The aim of this research was to derive an algorithm that predicts the winding pin capacity and occupancy as well as to develop a novel anchor that decouples the fiber net from the pin orientation.

Anchors

Point load application is a common task in the design of fiber-reinforced composites.[25] In the case of planar sandwich or monolithic[26] components, metallic inserts[27,28] are integrated during production[29,30] or subsequently attached[31,32] to a drilled hole.[33,34] Joint elements can also be attached to the component perimeter[35,36] or directly glued onto the surface.[37] Objects manufactured with CFW often already have such features, provided by the anchors, which can be used for load transmission. Therefore, during the design phase anchors for CFW can be divided into two groups: ones used later for load transmission and those that are used only for shaping the fiber arrangement by redirecting the fibers at a specific point in space. The remaining parts of the anchors are often metallic and can be used as a mechanical buffer when high forces are acting on the component. For example, a metallic sleeve can prevent the threads[38] of a bolt from damaging the composite in these cases. Another function that is performed by these elements is the tolerance compensation during assembly.[39]

There are several types of anchors, see Figure 1. The relevant parameters of the anchors are the price, maximum capacity, minimum bending radius, hold down feature for

fibers, reusability, compatible winding fixture materials, and if their constituents remain in the component.

Eyelets are almost never used, as they require the fibers to be threaded through them, which is not yet feasible in terms of an automated manufacturing process. The pin category includes slender, often cylindrical, protruding and attachable elements, around which the fibers are wound using a hooking motion. Sleeve/washer combinations[16] (see Figure 1 m and n), which can be fastened with an internal bolt, are most often used in CFW. The combination with metallic fixtures makes them suitable for high fiber tensions,[40] which are typical for large components. Release agents should be applied to washers and bolts. One advantage is that the washers prevent the fibers from sliding off, thus creating a more compact fiber strand.[41] A disadvantage of the washers is that they can cut filaments during contact while hooking motions, as well as the limited number of angles possible between the fiber and pin. If this angle range is exceeded, the fibers are deposited on the perimeter of the washers and the mechanical performance decreases significantly due to the kinking[42] of the fibers. The consequence is a geometrical dependency between the pin and fiber orientation, which imposes a geometric limit on the assembly configuration.[43] Nails and spikes can be used as pins without the hold down feature. These are typically attached to wooden fixtures and used with low fiber tension for small prototypes. Another type of element is hooks, which are undercuts, pockets, or indentations within the winding fixture or the component. The fibers are in contact with the edges of those undercuts.[17] No circular hooking motion can take place and fibers can be positioned from one side only. Grooves have similar features to those of hooks. The winding fixture or component contains elongated grooves on its surface, into which fibers are placed.[44] The depth, width, and orientation correspond to the fiber material used. The winding fixture can be 3D-printed or

Figure 2. First iteration of the adaptive winding pin. Top: regular configurations with 3 and 2 upwards facing arms. Bottom left: an irregular configuration with 3 arms. Bottom right: a configuration with 4 arms facing downwards.

grooves can be milled into a component.[45] The use of continuous surfaces to support fibers includes the edges and faces of the winding fixture, as well as freshly placed and already-cured fiber bundles.

Winding fixtures are defined by the way they hold the anchors in place. They can be made of metal, plastic, timber, or foam[46] by differential construction methods or milling. The criteria for the fixture selection are the cost, type of anchor, reusability of the fixture, maximum fiber tension, design freedom, and maximum curing temperature. Additional restrictions may apply if the fixture remains within the component.

Adaptive winding pin design

The developed anchor should allow fibers to be received from as many directions as possible to enable the volumetric design of CFW objects. The result of the development was an additive manufactured pin which uses a bolt connection. To be adjustable to any position within the fiber net, the complete CAD model of the winding pin was parameterized.

First iteration

The first iteration (see Figure 2) of the adaptive winding pin has a base containing a threaded hole in the bottom center. From this, a constricted pole extends upwards to a sphere.

From there, several arms pultrude in different directions, which can be adjusted to match the fiber net. At the end of each arm, a disc prevents fibers from slipping off. There is a measuring tip on the outward facing surface of each disc, enabling the position and alignment of the pin can be measured before and after winding. The measuring tip is inlaid in the contour so as to not damage fibers during winding. The fibers can be placed around the pin covering the arms, sphere, and pole so that only the outer surfaces of the discs and base remain uncovered. The entire pin stays in the component. It is disadvantageous that the base limits the bolt hole depth and the central sphere reduces the pin capacity, preventing a uniform fiber placement because of surface discontinuities, which was improved in the final iteration. This iteration of the pin should be used for prototyping.

Final iteration

In the final iteration of the winding pin, the threaded hole was incorporated up to the center of the pin and the sphere was eliminated to introduce rounding with a constant curvature, see Figure 3. As a result, the screw-in depth could be increased without lengthening the pin and thus its lever arm. Almost all the surface discontinuities could be removed, which improved the fiber deposition quality.[40] Additionally, a bottom-mounted 3D-printed adapter was introduced. It could be used to clamp the pin to profiles of a modular fixture system. The reusable adapter was attached to the pin via a grub screw by the already-existing central bolt hole and removed after curing the component. The adapter includes parallel clamping surfaces to fix the pin during preprocessing and contains a slot on the bottom to align the pin with a screwdriver during assembly. The base is hexagonally shaped to make it easier to clamp the pin and align it.

Geometric design parameters

The CAD model was driven by form-defining geometrical parameters: the height of the pin, the length of each arm, the horizontal and vertical angles of each arm, disc diameter D_i, arm diameter d_i, base diameter D_j, pole diameter d_j, and bolt size (see Figure 4). Additionally, the distances between the main winding point and the sub winding points could be set (compare to Figure 6). The parameters allow to adapt the geometry of each winding pin individually to match the fiber net configuration at its position. Hooking the fibers at the arms of the winding pin allows to decouple the orientations of the fiber net and the bolt connection.

Winding technique

Compared to a sleeve/washer winding pin, the complexity of the fiber hooking increased due to the higher number of
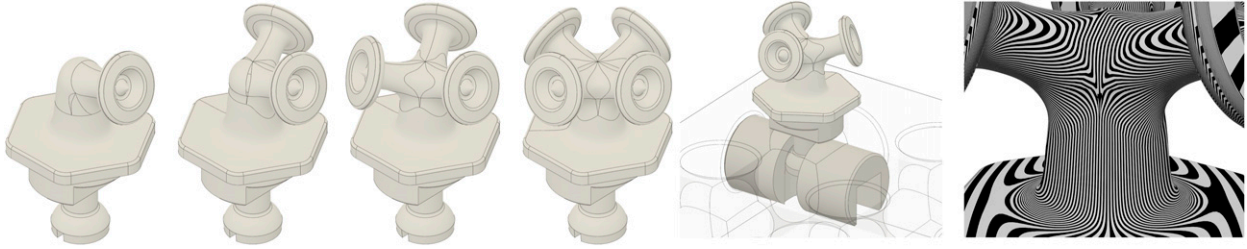
Figure 3. Final iteration of the adaptive winding pin. From left to right: several variants of the pin with 1, 2, 3, and 4 arms, including the adapter, the attachment to the profiles of the modular fixture system, and zebrastripe—analysis of a 3-arm configuration.

fiber placement possibilities. This allows fiber bundle alignments that are not perpendicular to the pole or arms. For example, the fiber can approach and depart the pin at the upper midpoint and hook around one of the arms from below. Fiber kinks caused by discs should be avoided by contacting the pin from orientations as far away from the discs as possible. Additionally, it is mechanically advantageous to place fiber bundles that are parallel to each other on the same side of a pin so that they are not separated. In general, the pin should be filled from the inside out and from the bottom up to minimize lever arms.

Additive manufacturing of the winding pin

The winding pin was produced by laser powder bed fusion (LPBF) using aluminum powder. An additive manufacturing process is the only feasible fabrication option because of the high geometrical complexity. Other materials such as titanium or stainless steel may be needed depending on the structural design. The use of plastics would be limited to low-performance applications. The pin surface has a high roughness set by the LPBF process parameters, see Figure 5. Therefore, relative movements between the filaments and the pin surface can damage the rovings. A smoothing post-process for all contact surfaces is not economically feasible. Sandblasting is effective but labor-intensive, whereas barrel tumbling produces unsatisfactory results on the relevant surfaces of the inner pin areas.[47] However, the use of a special winding technique[48,49] can prevent fiber damage, but its implementation in robotic systems remains an open challenge due to the required complexity of the trajectories. Another potential way to mitigate minor surface irregularities would be to apply a dip coating. This would create an additional interface between the fiber composite and the pin surface, which could affect load transmission. The orientation of the pin during the printing is of decisive importance, since this determines the areas where support structures are needed to realize overhangs. Areas with support structures have more surface imperfections and should preferably not be located where fibers are mainly placed. This aspect requires quality-enhancing advancements in the LPBF process, since coatings cannot compensate for such major imperfections.

Digital representation of the winding pin

To integrate the adaptive pin into the digital design process, it is represented as multiple regular sleeve/washer winding pins, see Figure 6. The total volume V_{env} that the fiber can occupy around adaptive pin, the fiber envelope, is calculated from the CAD model, see Figure 6. The top part of the volume is segmented according to the number and orientation of the arms of the adaptive pin. The decisive factor here is the smallest volume of each arm. Then, the same volume is assigned from the lower part of the pin to each arm. The remaining part V_j of the total volume is assigned to the pole. The diameters of the imaginary sleeves and washers are identified from the CAD design parameters of the pole, arms, base, and discs. The height of the imaginary sleeves can be calculated for each sub winding point by

$$h_{j,V} = \frac{4V_j}{\pi\left(D_j^2 - d_j^2\right)} \quad \text{and} \quad h_{i,V} = \frac{4V_i}{\pi\left(D_i^2 - d_i^2\right)}. \quad (1)$$

Alternatively, the sleeve/washer parameters can be calculated from the cross-sectional area of a cut of the fiber envelope in the angular orientation of each arm. In this case, the height of the imaginary sleeve of the pole can be calculated by $h_{j,A} = 2\,A_{\mathrm{bottom}}\left(D_j - d_j\right)^{-1}$. Applying this approach to the arm leads to an overestimation of the capacity. Therefore, the formula is modified:

$$h_{i,A} = \frac{1}{2}\left(h_{i,V} + \frac{2\,A_{\mathrm{top}}}{D_i - d_i}\right). \quad (2)$$

Winding syntax

The winding syntax[14] is a list of indicators of the winding points sorted by the chronological order in which the fiber is hooked onto the anchor of the winding point. The indicators are usually integers and refer to the winding point parameters (cartesian coordinates and orientation of the anchor). In the case of the adaptive winding pin, the winding syntax must be specified on the level of the sub winding points. The winding syntax defines the spatial arrangement of the fiber bundles between the anchors and the distances between anchors.
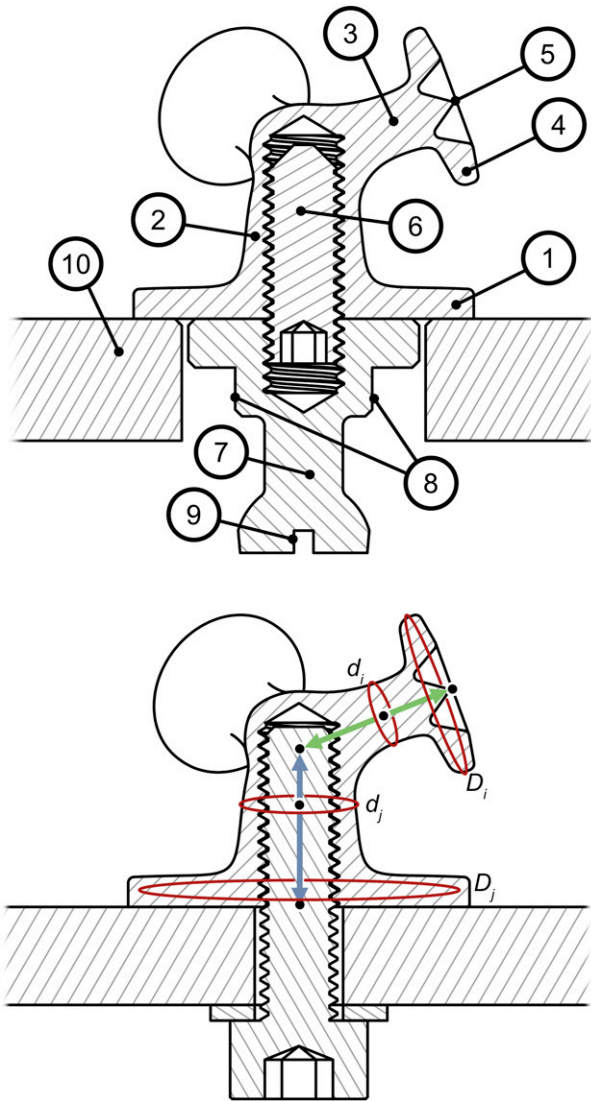
Figure 4. Cross-sectional views of the final iteration of the adaptive winding pin. Top: configuration of the pin mounted to the modular fixture system. 1: base; 2: pole; 3: arm; 4: disc; 5: measuring tip; 6: grub screw; 7: adaptor; 8: planer surfaces for clamping; 9: screwdriver slot; 10: profile of the modular fixture system. Bottom: configuration of the pin after winding and assembly, parameters of the CAD model: height of the pin (blue), length of the arm (green), horizontal and vertical angles of each arm, disc diameter D_i, arm diameter d_i, base diameter D_j, pole diameter d_j, and bolt size.

Hooking syntax and hooking condition

The hooking syntax of a pin describes the sequence in which fibers are hooked around it. It can be derived from the winding syntax and consists of a list of turns $(u, 1u = 360°)$ of the fiber and the direction the fiber is coming from (α). The additional amount of u, depending on the position where the fiber tangentially departs from the sleeve surface, is given as Δu and can be calculated as

Figure 5. Regular 3-arm adaptive winding pin made from aluminum and ready for winding. The underlaying profiles of the modular fixture system are covered by PTFE foil and the gap in between is protected by vacuum sealing tape. For the parameters of this pin, see Table 2.

$\Delta u = 0.5 - \pi^{-1} \arccos(2S/L)$. The hooking condition $H \in \mathbb{Z}$ is defined by the way the fiber bundle is wrapped around the pin, see Figure 7. It can be calculated from the turns:

$$H = \begin{cases} \lfloor u \rfloor, & \text{if} \quad u \bmod 1 \leq 0.5 \\ -\lfloor u \rfloor - 1, & \text{if} \quad u \bmod 1 > 0.5 \end{cases} \quad (3)$$

Winding pin capacity

The pin capacity is defined as the ability of the winding pin to absorb fiber bundles. It is depleted if the next hooking would result in fibers slipping off the pin. Therefore, the same pin can have different capacities depending on the hooking syntax. The maximum volume a pin offers to absorb fibers is given as $V_{\text{pin}} = \pi h (W^2 - S^2)$, with the radius of the washer W and the radius S and height h of the sleeve.

Winding pin occupancy model

The occupancy of the pin cannot just be approximated by the ratio sum of all fiber volumes and V_{pin}, since the capacity is reached before the entire volume is filled, see Figure 9. This results from a one-sided material deposition, as defined in the hooking syntax. In CFW, this is typical because fibers are often spanned between multiple clusters of anchors. In the following, an approximative model based on geometric parameters is derived into an algorithm to predict the winding pin occupancy, see Figure 8.

Since the algorithm is intended for early design phases, only a few parameters are known, such as the fiber net
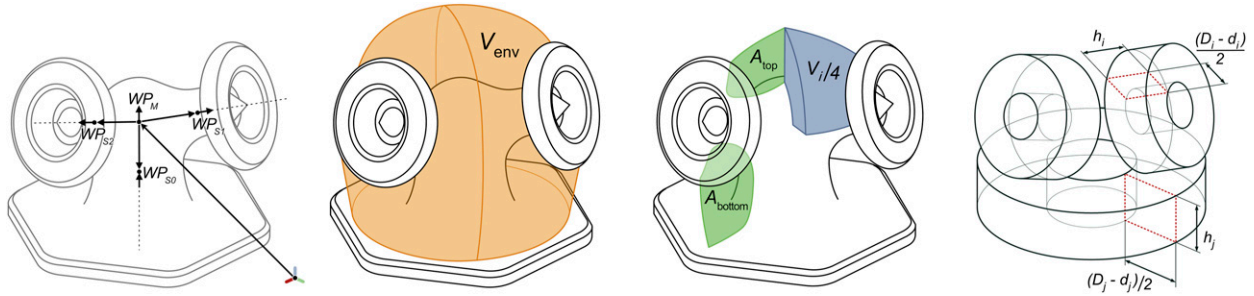
Figure 6. Method for converting the fiber envelope of the adaptive winding pin into a sleeve/washer equivalent. From left to right: identification of the sub winding points WPS, main winding point WPM, and their orientation unit vectors; complete fiber envelope (orange); identification of the cross-sectional areas (green) and minimum volume section (blue); representation of the winding pin as separate imaginary sleeve/washer configurations.
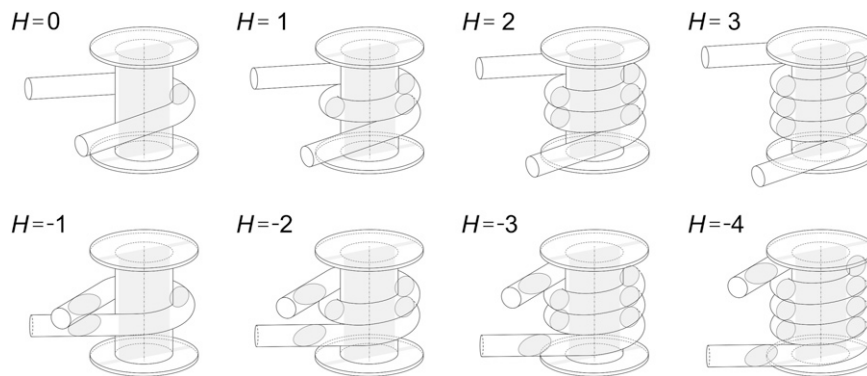

Figure 7. Exemplary visualization of different hooking conditions H.

configuration, winding pin geometry, and fiber properties. Therefore, the algorithm relies on a model that involves several simplifications. The most important one is the neglection of compression in the fiber composite caused by fiber tension. Its implementation would require comprehensive information about the dynamic behavior of the manufacturing equipment, which is highly dependent on the component geometry and the trajectory creation methods used. The second most relevant simplification is the assumption of a constant fiber volume ratio and the absence of voids. In CFW, the fiber volume ratio varies substantially along the fiber. The void content can be significant since in CFW consolidation is primarily generated by curvature. Incorporating these aspects would require a computational model of the impregnated fiber composite material interacting with the manufacturing system. Furthermore, geometric simplifications are made with respect to fiber interactions (fiber sliding and bending, deformations of bundles, and interaction beyond the washer perimeter) that would require a physics-based soft-body simulation.

From these simplifications, the hypotheses for the developed algorithm can be derived:

- The main hypothesis states that the calculation can be split into a first step, where fiber distribution is approximated based on volumes, and a second step, where the occupancy is evaluated based on hooking conditions and the pin cross-sectional area.
- The second hypothesis is that the fiber volume between the washers can be mapped to quantized concentric layers and assigned to a single angular position per winding step to sufficiently approximate the fiber accumulation.
- The third hypothesis states that the occupancy can be calculated by considering a single cross-sectional plane that intersects the winding pin at the angular position of the fiber distribution peak.
- The fourth hypothesis states that this angular position can be found by averaging the fiber distribution, similar to a center of gravity determination by using the fiber volumes as weighting factors and the layer distance from the center as lever arm.

The fiber bundle imaginary radius can be given in mm as $r = \sqrt{T/(\pi\ \varphi\ \rho)}$, with the linear density T in ktex, the fiber volume ratio φ of the composite, and the density ρ of the fiber in g/cm^3. The volume occupied by the fiber bundle around the sleeve can be calculated as a helix with a pitch of $2r$. Both ends of the helix are extruded until the perimeter of the washer is reached. The total fiber bundle volume can be calculated   as
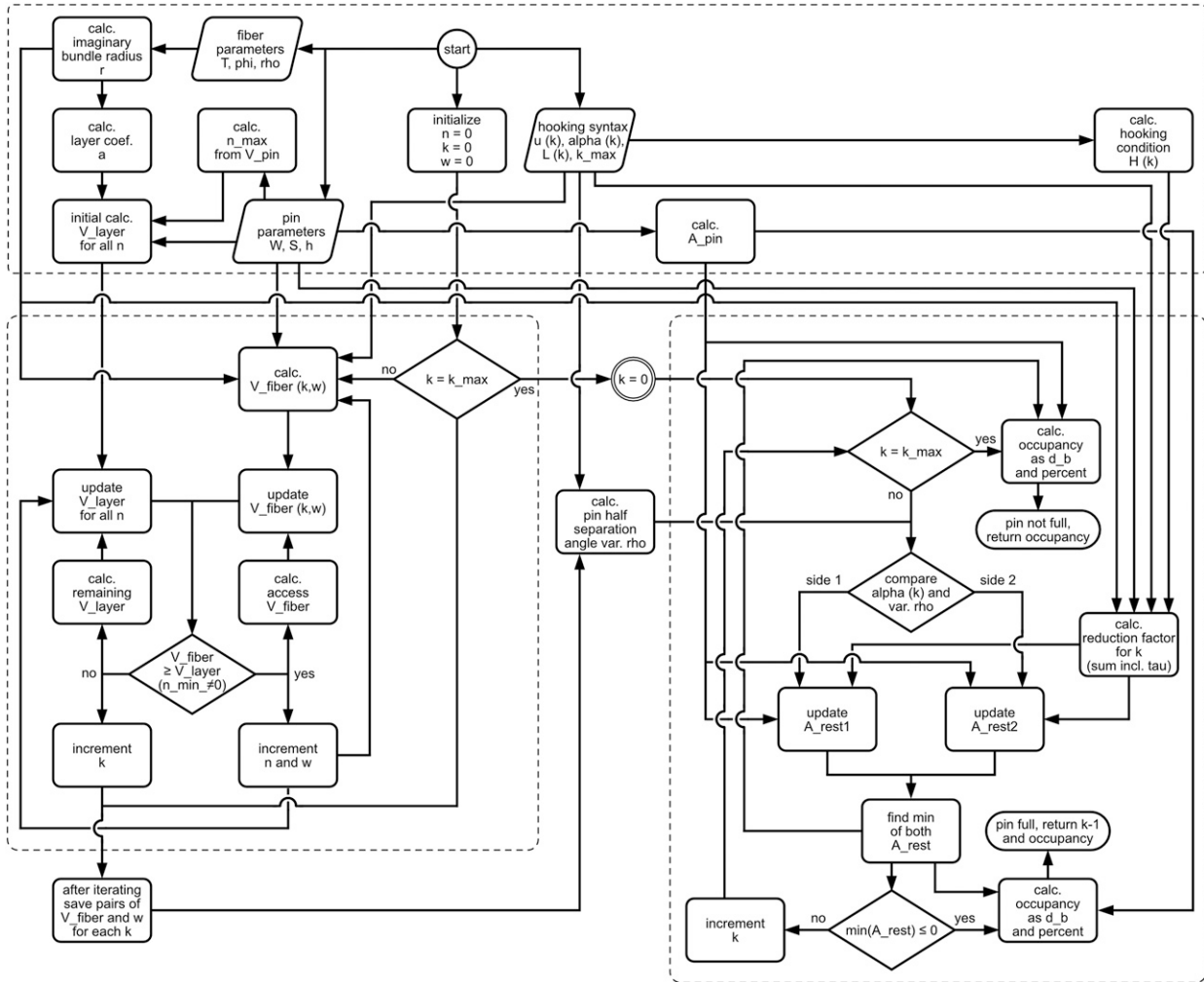
Figure 8. Flowchart of the winding pin occupancy model algorithm. The procedure consists of three domains, after the parameter initialization (top domain), the filling of the pin layers with fiber volumes is approximated in an iteratively procedure (bottom left domain), followed by a stepwise reduction of the cross-sectional pin areas to obtain the occupancy (bottom right domain). The label "sum incl. tau" refers to the right side of the equations (5) and (6).

$V_{\text{fiber}} = 2\,\pi\,r^2 \left(u\,\sqrt{\pi^2 R^2 + r^2} + \sqrt{W^2 - R^2} \right)$, with the number of turns u and $R = r + w + S$. If R is greater than W, the second square root is omitted. The radial distance w between the sleeve and fiber bundle surface is set for each step k of the hooking syntax. During winding, the pin is filled from the center up and down and from the inside out. To model this behavior, the pin volume is divided into concentric layers with the same thickness. The volume of the n-th layer can be calculated as $V_{\text{layer}} = \pi\,a\,h\,(2an - a + 2S)$, with $a = r\,\sqrt{\pi}$. Inner layers are filled first. Since w and the volume V_{fiber} of a fiber bundle are interdependent, the calculation must be iterative. After both parameters have been determined, the horizontal angle ϱ representing the most occupied half of the winding pin is calculated as $\varrho = \tan\left(\sum_k V_{\text{fiber}_k}\,w_k\,\sin(\alpha_k) / \sum_k V_{\text{fiber}_k}\,w_k\,\cos(\alpha_k) \right)$, with

the horizontal angle α between the bisecting plane between both fibers and the main axis of the pin. After ϱ is known, each fiber hooking is assigned to one of the pin halves based on α. Each half is represented by the cross-sectional pin area $A_{\text{pin}} = h\,(W - S)$. For each step k of the hooking syntax, $\pi\,r^2$ is subtracted from A_{pin1} or/and A_{pin2} according to the hooking condition H, the distance between winding points L, and the scaling factor τ for negative hooking conditions:

$$\tau = \begin{cases} 2\pi\,\arcsin(2S/L), & \text{if } H < 0 \\ 1, & \text{otherwise} \end{cases} \quad (4)$$

$$A_{\text{rest1}} = A_{\text{pin1}} - \sum_k \begin{cases} \pi\,r^2\,(|H_k + 0.5| + 0.5), & \text{if } \alpha_k \in [\varrho - 90°, \varrho + 90°] \\ \pi\,r^2\,\tau_k\,|H_k|, & \text{otherwise} \end{cases}$$

$$(5)$$

$$A_{\text{rest2}} = A_{\text{pin2}} - \sum_k \begin{cases} \pi \, r^2 \, \tau_k \, |H_k|, & \text{if } \alpha_k \in [\varrho - 90°, \varrho + 90°] \\ \pi \, r^2 \, (|H_k + 0.5| + 0.5), & \text{otherwise} \end{cases}$$

$$(6)$$

$$A_{\text{rest}} = \min(A_{\text{rest1}}, A_{\text{rest2}}) \qquad (7)$$

If A_{rest} falls below zero, the winding pin capacity is fully utilized and the occupancy exceeds 100%.

To visualize the fiber net, the bundle diameter of each edge between two nodes (anchors) can be inserted to its corresponding position in the adjacency matrix[50] of the winding object. To implement information on the winding pin occupancy, the diameter $d_b = 2\sqrt{(A_{\text{pin}} - A_{\text{rest}})/\pi}$ can be incorporated in the diagonal of this matrix.

Results and discussion

The results of the occupancy model algorithm were experimentally tested in different hooking scenarios with relevance for CFW. Typically, a CFW component is built up between two or more winding pin clusters, often arranged in space in symmetrical patterns. Alternatively, for planar components, the pins are mounted in parallel orientation on a base plate. The clustering results in a classification of two common fiber net configurations at anchors. In the first one, the pin has several fiber connections oriented towards the center of the component, often in two or more distinct directions. This can be combined with an edge reinforcement that runs along the perimeter of the component and therefore connects to the pin roughly perpendicular to the other fibers. In the other common type of fiber net configuration, the winding pin is located inside the component and its main purpose is fiber deflection. Here, the fiber orientations are more diverse, but the number of turns is lower. These characteristics helped to identify the relevant cases for the experimental tests. The capacity of different sleeve/washer and adaptive winding pins were investigated in manual winding, see Figure 9. The aim of these experimental tests was to verify the reliability of the algorithm for relevant CFW cases. Structural investigations are beyond the scope of this study. The ratio between fiber and pin size was chosen based on an application-oriented range. Extreme ratios would have biased the results by overemphasizing the influence of neglected effects, see section on the winding pin occupancy model. Therefore, a capacity of the winding pins in the tens range was selected for the tests. A single Tenax-E 24K STS40 F13 carbon fiber roving[51] with $T = 1600$ tex and $\rho = 1.78$ g/cm³ together with an aliphatic epoxy resin[52] was used. Based on pyrolysis measurements[40] of this material, φ was set to 51.9% for the calculation. Determining the remaining capacity of a partially filled winding pin is very inaccurate in the real world. Therefore, in the experiment, the number of hooking syntax repetitions to completely fill the winding pin was counted

rather than the occupancy after a certain number of repetitions. Variations in experimental results were mitigated by testing each case several times and rounding the median to

Figure 9. Experimental testing of the occupancy algorithm for several non-trivial cases, see Table 1 and 3. Top: Sleeve/washer winding pin test case 4, the pin is completely filled as further addition of fibers would create an instable fiber accumulation. Middle: Sleeve/washer winding pin test case 5 (left pin) and case 12 (right pin), the left pin is not completely filled while the right one is, although in both cases the pin volume is not fully occupied. In the right pin fibers are about to slip over the edge of the washer at the lateral areas. Bottom: 3-arm winding pin test case 3, although only the pole and the arm in the front received fibers, the capacity of the whole pin is exhausted at this hooking step.

Table 1. Winding pin occupancy model validation results for sleeve/washer pins.

Case	Hooking syntax (turns u, orientation α, repetitions b, j, and pin distance L [mm])	$s_s = 0.816$ $A_{pins} = 19.6$		$s_m = 0.485$ $A_{pinm} = 33$		$s_g = 1.212$ $A_{ping} = 82.5$		$s_l = 5.000$ $A_{pinl} = 28.8$	
		j_{exp}	j_{sim}	j_{exp}	j_{sim}	j_{exp}	j_{sim}	j_{exp}	j_{sim}
1	$u = [j] * 1$, $\alpha = [0°] * 1$, $L = [0] * 1$	10	10	18	18	44	46	17	15
2	$u = [0.25] * j$, $\alpha = [0°] * j$, $L = [50] * j$	13	11	20	19	52	47	22	16
3	$u = [0.5] * j$, $\alpha = [0°] * j$, $L = [50] * j$	11	11	20	19	50	47	20	16
4	$u = [1.5 + \Delta u] * j$, $\alpha = [0°] * j$, $L = [100] * j$	12	10	18	18	44	45	20	15
5	$u = 0.5 + \Delta u * j$, $\alpha = [0°] * j$, $L = [50] * j$	10	10	18	18	44	47	18	16
6	$u = [0.75] * j$, $\alpha = [0°] * j$, $L = [50] * j$	11	10	17	17	30	43	18	14
7	$u = [1] * j$, $\alpha = [0°] * j$, $L = [50] * j$	6	5	9	9	20	23	8	8
8	$u = [1.5] * j$, $\alpha = [0°] * j$, $L = [50] * j$	5	5	9	9	25	23	10	8
9	$u = [1.5 + \Delta u] * j$, $\alpha = [0°] * j$, $L = [100] * j$	5	5	9	9	21	23	11	8
10	$u = [1.5 + \Delta u] * j$, $\alpha = [0°] * j$, $L = [50] * j$	5	5	9	9	17	23	11	8
11	$u = [2] * j$, $\alpha = [0°] * j$, $L = [50] * j$	4	3	7	6	12	15	7	5
12	$u = [\Delta u, \Delta u] * j$, $\alpha = [0°, 180°] * j$, $L = [50] * j$	10	11	15	19	21	47	11	16
13	$u = [\Delta u, \Delta u] * b + [0.5] * j$, $\alpha = [0°, 180°] * b + [0°] * j$, $L = [50, 50] * b + [50] * j$	$b = 5$		$b = 8$		$b = 11$		$b = 6$	
		6	6	12	11	24	36	11	10
14	$u = [0.5, 0.5] * j$, $\alpha = [0°, 180°] * j$, $L = [50] * j$	6	11	10	19	19	47	6	16

ones. These variations are caused by compression resulting primarily from variations in fiber tension, which are characteristic of both manual and robotic CFW. The samples were produced manually using a passively tension-controlled creel and a cartridge-based direct impregnation system.[16] The winding pins were mounted to a stainless-steel base plate with a grid of threaded holes or the modular winding fixture. After winding, each case was replicated using the algorithm and its prediction (j_{sim}) was compared with the counted repetitions from the experiment (j_{exp}), see Table 1 and 3.

Model validation for sleeve/washer winding pins

Sleeve/washer winding pins with different parameters ($S_s = 4$ mm, $W_s = 8.9$ mm, $h_s = 4$ mm; $S_m = 4$ mm, $W_m = 12.25$ mm, $h_m = 4$ mm; $S_g = 4$ mm, $W_g = 12.25$ mm, $h_g = 10$ mm; $S_l = 5$ mm, $W_l = 7.4$ mm, and $h_l = 12$ mm) were used, each with a slenderness $s = h/(W - S)$. Table 1 compares the experimentally (j_{exp}) determined and the calculated (j_{sim}) repetitions for several cases and pins.

Case 1 represents the filling of the pin as conducted with a cable drum. Case 2 and 3 ($H = 0$) are, together with cases 4–6 ($H = -1$), the most used scenarios in the CFW design process. Cases 8–10 are similar but contain an extra wrapping of the pin. Cases 7 and 11 represent a wrapping of a tangentially bypassing fiber. A sin/cos reinforcement is investigated in case 12, together with subsequent hooking with condition 0 in case 13. Case 14 presents the alternating hooking from antipodal orientations, something which is remote from a CFW application.

In general, the algorithm shown in the section on the winding pin occupancy model predicts the capacity of the sleeve/washer winding pins sufficiently well for the design process. For $H = 0$, the algorithm slightly underestimates the pin capacity; in case 12, it overestimates it, and in the other ones it depends on the pin. The prediction of the capacity for cases with $H = -1$ depends on the correct reduction performed by τ. From cases 4 and 5 as well as 9 and 10, it can be seen that the distance influence is only recognizable for pins with a larger capacity and that the algorithm does not represent this particularly well. Cases with a positive H are independent of this. Cases 7–10 correctly show the same predicted values. Cases 12 and 13 show that the prediction is significantly better if the pin is only partially filled with a sin/cos reinforcement. The reason for this is that fiber–fiber interactions are more prominent in case 12. The same effect is seen in case 14, where the capacity is overestimated by 120% on average. This results from the calculation of ϱ, which is based on the occupancy of the pin in the fiber direction and not the fiber–fiber interaction at $\varrho \pm 90°$. In addition, a longer hooking condition ($u = [0.5] * 7j$, $\alpha = [0°, 315°, 270°, 180°, 90°, 153°, 116°] * j$, $L = [100, 71, 112, 100, 50, 112, 112] * j$) was tested with a sleeve/washer pin ($s_m = 0.485$, $A_{pinm} = 33$), showing the same behavior of the algorithm: 3.2 experimental repetitions to 4.9 by simulation.

Pin m was predicted most accurately and pin s also showed only small deviations, since for both the capacity war primarily geometrically determined. For pins with a larger A_{pin}, the fiber accumulation can be more easily compacted by an increase in fiber tension. Even without any fiber crossing coming from negative H or crossing multiple fibers, in those pins there is an influence of the fiber–fiber interactions between radial layers. In contrast, pin l was

Table 2. Geometrical parameters of the tested adaptive winding pin digital representations.

Calculation method	Pin parameter (arm i, pole j)	2-arm pin (110° separation)	3-arm pin (regular)	
Max. fiber envelope from CAD	V_{env}	1771.322	1715.687	mm³
CAD pin design parameter	D_i	8.400	8.400	mm
CAD pin design parameter	d_i	3.200	3.200	mm
Assigned section of envelope	V_i	284.404	325.284	mm³
Calc. based on D_i, d_i and V_i	$h_{i,V}$	6.003	6.866	mm
CAD pin design parameter	D_j	15.000	15.000	mm
CAD pin design parameter	d_j	5.810	5.810	mm
Calc. based on V_i and V_{env}	V_j	1202.514	739.835	mm³
Calc. based on D_j, d_j and V_j	$h_{j,V}$	8.053	4.954	mm
Envelope cross-section (top)	A_i	18.644	18.466	mm²
Calc. based on D_i, d_i, A_i, and $h_{j,V}$	$h_{i,A}$	4.737	5.168	mm
Envelope cross-section (bottom)	A_j	28.686	29.342	mm²
Calc. based on D_j, d_j, and A_j	$h_{j,A}$	6.267	6.411	mm

Table 3. Winding pin occupancy model validation results for adaptive pins.

Pin type	Hooking syntax (turns u, orientation α, repetitions at arms i, repetitions at the pole j and pin distance L [mm])	Pole			Arm(s)		
		j_{exp}	$j_{sim,V}$	$j_{sim,A}$	i_{exp}	$i_{sim,V}$	$i_{sim,A}$
2-arm pin (110° separation)	Pole only $\quad u = [0.5] * j, \alpha = [55°] * j, L = [167] * j$	17	21	16			
	Arms (horiz.) $\quad u = [0.5, 0.5] * i, \alpha = [55°, 55°] * i, L = [167, 167] * i$				8	9	7
	Pole + arms $\quad u = [0.5] * j + [0.5 + \Delta u] * 2 i, \alpha = [55°] * j + [55°] * 2 i, L = [167] * j + [167] * 2 i$	16	21	16	6	8	6
	Arm (radial) $\quad u = [0.5] * i, \alpha = [0°] * i, L = [167] * i$				7	9	7
3-arm pin (regular)	Pole only $\quad u = [0.5] * j, \alpha = [60°] * j, L = [167] * j$	18	13	16			
	Arm (horiz.) $\quad u = [0.5 + \Delta u] * i, \alpha = [60°] * i, L = [20] * i$				7	9	7
	Pole + arm $\quad u = [0.5] * j + [0.5 + \Delta u] * i, \alpha = [60°] * j + [60°] * i, L = [167] * j + [20] * i$	19	13	16	6	9	7
	Arm (radial) $\quad u = [0.5] * i, \alpha = [0°] * i, L = [167] * i$				7	10	7

underestimated, which was caused by its uncharacteristic high slenderness. This allowed fibers in reality to accumulate more easily at the vertical pin center without the need for washers to prevent fiber slippage. With an increased slenderness, the influence of the axial positioning of fibers and axial dislocation, defined by fiber vectors and friction, increases. In the design process, an underestimation of the capacity is conservative.

Model validation for adaptive winding pins

Based on the method described in the section on the digital representation of the winding pin, the parameters for two different configurations of the adaptive winding pin were calculated, see Table 2.

With the same material and algorithm as that used in the previous section, the capacity of the 2-arm and 3-arm pin was predicted, see Table 3.

Both pins were tested in four cases. In the first one, the hooking was performed at the pole only. In the second, the fibers were spanned horizontally between the arms in such a way that they passed over the pin center, as mentioned in the section on the winding technique. For the 2-arm pin, both arms were used, whereas with the other one only one was filled. In the third case, the pole and then subsequently the arms were filled with the same hooking condition as that in case two. In the last case, only one arm was filled, with radial fibers attaching orthogonally from the arm axis.

Two methods for converting the adaptive pin geometry into a sleeve/washer equivalent were tested. For the tested hooking syntaxes, the method depending on the cross-sectional area performed better and, in contrast to the volume-based method, tended to underestimate rather than overestimate the capacity. The prediction made by the volume-based method was more accurate for the pole than for the arms. The area-based method also performed well in cases where the pole and arms were both filled. Therefore, the total fiber envelope can be divided and assessed for the sub winding points separately.

For both types of winding pins, the model performed sufficiently to be used as a design tool for CFW. Therefore, the underlying hypotheses can be considered as sufficiently confirmed in this context. The justification for this

method is twofold: The calculation only relies on parameters (material and geometry) which can be easily obtained even in early design phases and the calculation time is around 100 milliseconds per pin. A highly detailed physics–based soft-body simulation of the fiber–fiber, fiber–pin, and fiber–equipment interaction potentially predicts the occupancy more precisely, but it involves the consideration of many parameters (see simplifications in the section on the winding pin occupancy model) and has to model numerous contacts between entities. Most of those parameters are unknown during the design phase.

Conclusions

The developed adaptive winding pin was deployed in laboratory-scale winding sessions to verify its design idea. The pin allows one to attach fibers from various directions without fiber kinks and removes the dependency between the pin orientation and the fiber net. By parameterizing the winding pin geometry, the individual orientation of each arm can be easily adapted to the local fiber net configuration of the pin position in the component. By using LPBF, each winding pin can be made in a unique shape at no additional costs. This is the prerequisite for each winding pin to be individually tailored to the structural requirements of the fiber net. This could lead to higher performing CFW structure in the future. The adaptive winding pin eliminates some design restrictions and allows the material to be placed only where it is needed. The multiple contact areas within a single adaptive pin facilitate a fiber placement which is more appropriate for the material due to the larger bending radius. This can help to prevent failure close to the pin, allows one to separate or merge fiber bundles, and also opens up more complex hooking syntaxes that are yet to be researched. This more homogeneous fiber arrangement could reduce variations in the structural performance. It was shown that the fiber should preferably be attached to an arm from the inside of the pin, rather than the outside. An adaptive pin is a prerequisite for voluminous, sparse, and fully stressed framework structures. However, the price of the metallic additive manufacturing limits the industrial application of the pin at large scales or in large quantities. The use of the modular fixture system in combination with the winding pin adapters helps to shorten the preparation time of the winding sessions without sacrificing geometric accuracy. The only drawback is that pin positions are mainly restricted to a grid. The winding pin capacity model can be used for relevant hooking syntaxes and typical winding pin geometries. It can also sufficiently be applied to the adaptive pin. Due to its integration in digital process planning tools, the pin capacity can be directly assessed during the early design phases, which is another step towards the realization of a fully automated CFW process chain.

Author contributions

Pascal Mindermann: Conceptualization, Methodology, Software, Validation, Formal analysis, Investigation, Data Curation, Writing - Original Draft, Writing - Review and Editing, Visualization, Project administration, Funding acquisition;

Götz T. Gresser: Validation, Resources, Supervision.

Declaration of conflicting interests

The authors declared no potential conflicts of interest with respect to the research, authorship, and/or publication of this article.

Data availability statement

Data is contained within the manuscript.

ORCID iDs

Pascal Mindermann 📷 https://orcid.org/0000-0002-6929-9026
Götz T. Gresser 📷 https://orcid.org/0000-0001-5501-2912

References

1. Prashanth S, Subbaya KM, Nithin K, et al. Fiber reinforced composites – A review. *J Mater Sci Eng* 2017; 6: 3.
2. Krebs F, Larsen L, Braun G, et al. Design of a multifunctional cell for aerospace CFRP production. *Int J Adv Manuf Technol* 2016; 85: 17–24.
3. Rubino F, Nistico A, Tucci F, et al. Marine application of fiber reinforced composites: a review. *J Mar Sci Eng* 2020; 8(1): 26.
4. Fairuz AM, Sapuan S, Zainudin ES, et al. Polymer composite manufacturing using a pultrusion process: a review. *Am J Appl Sci* 2014; 11(10): 1798–1810.
5. Schindler S, Bauder HJ, Wolfrum J, et al. Engineering of three-dimensional near-net-shape weave structures for high technical performance in carbon fibre–reinforced plastics. *J Eng Fiber Fabrics* 2019; 14: 1–16.
6. Arrabiyeh PA, May D, Eckrich M, et al. An overview on current manufacturing technologies: processing continuous rovings impregnated with thermoset resin. *Polym Compos* 2021; 1: 26.
7. Bodea S, Mindermann P, Gresser GT, et al. Additive manufacturing of large coreless filament wound composite

elements for building construction. *3D Print Addit Manuf.* Epub ahead of print 11 August 2021. DOI: 10.1089/3dp.2020. 0346.

8. Bodea S, Zechmeister C, Dambrosio N, et al. Robotic coreless filament winding for hyperboloid tubular composite components in construction. *Automat Constr* 2021; 126: 103649.

9. Estrada RD, Kannenberg F, Wagner HJ, et al. Spatial winding: cooperative heterogeneous multi-robot system for fibrous structures. *Constr Robot* 2020; 4: 205–215.

10. Quanjin M, Rejab M, Idris M, et al. Robotic filament winding technique (RFWT) in industrial application: a review of state of the art and future perspectives. *Int Res J Eng Tech* 2018; 5: 12.

11. Früh N and Knippers J. Multi-stage filament winding: integrative design and fabrication method for fibre-reinforced composite components of complex geometries. *Comp Struc* 2021; 268: 113969.

12. La Magna R, Waimer F and Knippers J. Coreless winding and assembled core – novel fabrication approaches for FRP based components in building construction. *Constr Build Mat* 2016; 127: 1009–1016.

13. Selvarayan SK, Krätschmer A, Hamm C, et al. Manufacturing of continuous fiber reinforced hierarchical compsite structures inspired by diatoms. In: *Euro Bio-inspired Materials*. Germany: Potsdam; 2016.

14. Zechmeister C, Bodea S, Dambrosio N, et al. Design for long-span core-less wound, structural composite building elements. In: *Impact: Design with All Senses*. Berlin, Germany: Springer; 2020, pp. 401–415.

15. Dreißig D, Faßbänder P and Hindenlang U. Simulation of carbon-roving-structures – extreme light and strong by filament wound reinforcement. In: 6th BETA CAE International Conference, Thessaloniki, Greece, 10–12 June 2015.

16. Mindermann P and Gresser GT. Robotic 3D deposition of impregnated carbon rovings with gradient properties for primary structures. In: 69th International Astronautical Congress, Bremen, Germany, 1–5 October 2018, Paris: IAF.

17. Büchler D, Elsken R, Glück N, et al. Ultraleichte raumzelle – Entwicklung von ultraleichten Großstrukturen in Faserverbund- und Hybridbauweise für den Schiffbau. In: *Statustagung Schifffahrt und Meerestechnik*. Germany: Rostock-Warnemünde; 2011, pp. 25–46.

18. Gil Pérez M, Rongen B, Koslowski V, et al. Structural design, optimization and detailing of the BUGA fibre pavilion. *Int J Space Struc* 2020; 35(4): 147–159.

19. Christie J, Bodea S, Solly J, et al. Filigree shell slabs – material and fabrication-aware shape optimisation for CFRP coreless-wound slab components. In: AAG2020, Paris, France, 28–29 April 2021.

20. Minsch N, Müller M, Gereke T, et al. 3D truss structures with coreless 3D filament winding technology. *J Comp Mat* 2019; 53: 2077–2089.

21. Bodea S, Dambrosio N, Zechmeister C, et al. BUGA fibre pavilion: towards robotically-fabricated composite building structures. In: Fabricate 2020, Online, 09–12 September 2020. London: UCL Press, pp. 234–245.

22. Dambrosio N, Zechmeister C, Bodea S, et al. Buga fibre pavilion – towards an architectural application of novel fiber composite building systems. In: Acadia 2019 – Ubiquity and Autonomy, Austin, USA, 24–26 October 2019.

23. Woods BK, Hill I and Friswell MI. Ultra-efficient wound composite truss structures. *Comp A* 2016; 90: 111–124.

24. Park KH and Lee YS. Implementation of automation program and efficient cable drum schedule using dynamic programming algorithm. *J Digit Contents Soc* 2016; 17: 4.

25. Kelly G. Load transfer in hybrid (bonded/bolted) composite single-lap joints. *Comp Struc* 2005; 69: 35–43.

26. Grezesik B, Mindermann P, Linke S, et al. Alignment mechanism and system concept of a scalable deployable ultra-lightweight space telescope for a 1U CubeSat demonstrator. In: 68th International Astronautical Congress, Adelaide, Australia, 25–29 September 2017, Paris: IAF, p. x38992.

27. Muth M, Schwennen J, Bernath A, et al. Numerical and experimental investigation of manufacturing and performance of metal inserts embedded in CFRP. *Prod Eng* 2018; 12: 141–152.

28. Falconieri D and Franco F. The effect of titanium insert repairs on the static strength of CFRP coupons and joints. *Comp Struc* 2015; 134: 799–810.

29. Lim JW and Lee DG. Development of the hybrid insert for composite sandwich satellite structures. *Comp Part A* 2011; 42: 1040–1048.

30. Song KI, Choi JY, Kweon JH, et al. An experimental study of the insert joint strength of composite sandwich structures. *Comp Struc* 2008; 86: 107–113.

31. Ekh J and Schön J. Load transfer in multirow, dingle shear, composite-to-aluminium lap joints. *Comp Sci Tech* 2006; 66: 875–885.

32. Camanho P, Tavares C, De Oliveira R, et al. Increasing the efficiency of composite single-shear lap joints using bonded inserts. *Comp B* 2005; 36: 372–383.

33. Wu CQ, Gao GL, Li HN, et al. Effects of machining conditions on the hole wall delamination in both conventional and ultrasonic-assisted CFRP drilling. *Int J Adv Manuf Tech* 2019; 104: 2301–2315.

34. Aamir M, Tolouei-Rad M, Giasin K, et al. Recent advances in drilling of carbon fiber–reinforced polymers for aerospace applications: a review. *Int J Adv Manuf Tech* 2019; 105: 2289–2308.

35. Zhu X, Liu Y, Wang Y, et al. Mechanical behavior of CFRP lattice core sandwich bolted corner joints. *Appl Comp Mater* 2017; 24: 1373–1386.

36. Vasiliev VV, Barynin VA and Razin AF. Anisogrid composite lattice structures – development and aerospace applications. *Comp Struc* 2012; 94(3): 1117–1127.

37. Pfeiffer E, Reichmann O, Ihle A, et al. Compact and stable earth deck multi-beam ka- band antenna structure and dual gridded reflector. In: 5th European Conference on Antennas and Propagation, Rome, Italy, 11–15 April 2011, New York: IEEE.

38. Hizam RM, Manalo AC, Karunasena W, et al. Effect of bolt threads on the double lap joint strength of pultruded fibre reinforced polymer composite materials. *Constr Build Mater* 2018; 181: 185–198.

39. Mara V and Kliger R. An approach to the development of connections between fibre reinforced polymer bridge decks. *Case Stud Struc Eng* 2016; 5: 18–26.

40. Mindermann P, Bodea S, Menges A, et al. Development of an impregnation end-effector with fiber tension monitoring for robotic coreless filament winding. *Processes* 2021; 9(5): 806.

41. Cerqueira J, Faria H and Funck R. Fabrication of composite cylinders with integrated lattice structure using filament winding. In: 16th European Conference on Composite Materials, Seville, Spain, 22–26 June 2014.

42. Wang Y, Chai Y, Soutis C, et al. Evolution of kink bands in a notched unidirectional carbon fibre-epoxy composite under four-point bending. *Comp Sci Tech* 2019; 172: 143–152.

43. Gil Pérez M, Dambrosio N, Rongen B, et al. Structural optimization of coreless filament wound components connection system through orientation of anchor points in the winding frames. In: IASS Annual Symposium 2019 – Structural Membranes, Barcelona, Spain, 7–10 October 2019.

44. Buragohain M and Velmurugan R. Study of filament wound grid-stiffened composite cylindrical structures. *Comp Struc* 2011; 93(2): 1031–1038.

45. Brymerski W, Fuhr JF and Nezami F. Additiv gefertigtes dachrahmensegment mit lokaler C-faserverstärkung. *Lightweight Des* 2019; 4: 52–55.

46. Kovaleva D, Gericke O, Kappes J, et al. Rosenstein pavilion: design and structural analysis of a functionally graded concrete shell. *Struc* 2019; 18: 91–101.

47. Mindermann P, Müllner R, Dieringer E, et al. Design of fiber-composite/metal–hybrid structures made by multi-stage coreless filament winding. *Appl Sci* 2022; 12: 2296.

48. Mindermann P, Witt MU and Gresser GT. Pultrusion-winding: a novel fabrication method for coreless wound fiber-reinforced thermoset composites with distinct cross-section. *Comp Part A* 2022; 154: 106763.

49. Mindermann P, Gresser GT and Milwich M. Method and tool arrangement for producing a fibre matrix composite profile structure and fibre matrix composite profile structure. Germany Patent EP000003808547A1, 2020.

50. Bapat RB. Adjacency matrix. In: Bapat RB (ed) *Graphs and Matrices*. London: Springer; 2010, pp. 25–44.

51. Teijin. *Tenax Filament Yarn. Product Data Sheet (EU)*; 2020. Available at: https://www.teijincarbon.com/fileadmin/PDF/Datenblätter_en/Product_Data_Sheet_TSG01en__EU_Filament_.pdf (accessed 3 December 2021).

52. *Bio-Composites and More GmbH*. PTP-resins. Available at: https://bio-composites.eu/en/ptp-resins/ (2021, accessed 3 December 2021).